Exploring and modeling radio signal propagation effects using ADS-B signals

Marc Kraft
(kraft@rhrk.uni-kl.de)

Markus Espen
(mespen@rhrk.uni-kl.de)

Mischa Helfenstein
(helfenst@rhrk.uni-kl.de)

February 2022

Abstract

Although the phenomenon of multipath propagation and the associated problems have been known for years, no reliable detection or mitigation strategy exists to this date. The characteristics of multipath propagation imply a difficult detection and an almost impossible mitigation of its effects. Since multipath propagation, at least in the aviation domain, is mostly environment-dependent, a model was developed which determines the influences of location-independent effects, such as the influence of the sensor, the fixed but unknown transmission power of the transmitter, as well as the unknown antenna position of the transmitter by means of various developed calibration algorithms, in order to identify geographical clusters of deviations. The analysis of a data set provided by SeRo Systems[1] revealed two interesting patterns, beam-shaped deviations of the signal strength around the sensor and ring-shaped deviations at medium distance around a sensor, which seem to be related to large concrete surfaces in close proximity to the sensors.

[1] https://sero-systems.de/

Contents

List of Figures

List of Tables

1 Introduction

The communication infrastructure in aviation is constantly evolving to enable secure and robust communications with high efficiency and accuracy. However, phenomenons persist on the underlying transport channel, wireless communication via radio waves, which can result in safety-critical problems at higher levels. One of these phenomenons is multipath propagation. In wireless communication, multipath propagation describes the phenomenon that occurs when a signal is received from multiple paths. Reasons for these multiple paths include various types of reflections, such as atmospheric ducting, ionospheric reflection, or simple reflections from buildings, mountains, etc., but also other influences on the propagation of a signal, such as refraction [10, 12, 17]. All these reflections or refractions can lead to different paths of a single signal, which are received with a time delay due to different velocities or different distances covered. Depending on the time offset of the reception of these different paths, these waves can interfere, constructively or destructively depending on their phase difference, or be received as independent signals. In the first case, constructive interference has an additive effect on the amplitude of the signal and amplifies it, while destructive interference attenuates the signal. In the worst case, this destructive interference can degrade signals to the point where they can no longer be detected and processed. The second case, receiving one or more paths of a signal as different, but identical signals, can also lead to many different problems at higher levels. Although this phenomenon and the problems associated with it have been known for many years, there is no clear solution. This is due to the fact that the impact of multipath propagation is hard to detect and harder to mitigate. Nevertheless, the drivers for multipath propagation are environmental and thus the corresponding impacts on signals should be relatively consistent in a geographic area that does not vary or varies only slightly.

Based on this assumption, the goal of this work is to develop a model that uses known influences on signal strength, such as propagation-induced attenuation, influence of the transponder's transmitter, and influence of the sensor and it's antenna, to identify geographic areas in which the received signal strength consistently deviates from the signal strength calculated by the model. The geographic areas identified by this method can then be examined in more detail for the characteristics of multipath propagation.

2 Model development

In aviation, transponders are a core component used by aircraft to communicate with each other and with ground stations. These transponders operate in different modes, which in turn can transmit different information. Mode-S, short for Mode-Selective, is the latest of these operating modes and enables, for instance, selective interrogations. Mode S Extended Squitter (1090ES ADS-B) transponders, which are the de-facto standard transponder for large aircraft, extend the functionality of Mode S with periodically broadcasted messages. [1][14] In this work we use a data set of collected extended squitter messages, more precisely airborne position messages, to model the effects of multipath propagation on aviation communication to identify geographic clusters of deviations.

2.1 Influences on a received signal due to multipath propagation

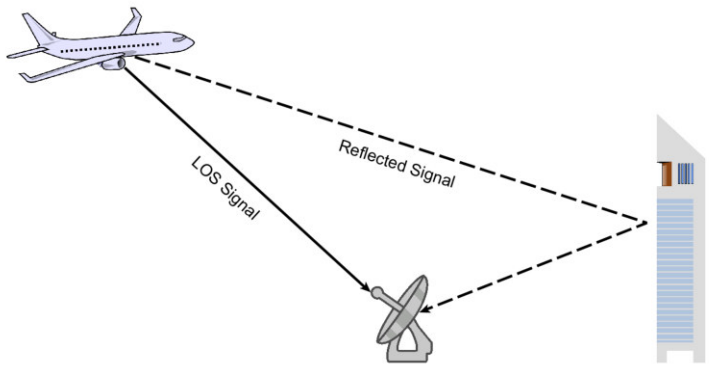

Figure 1: Broadcasted aircraft signal received multiple times from the same sensor.

Multipath propagation describes the phenomenon of radio signals being received not only by line of sight (LOS) propagation from transmitter to receiver, but also by reflections, diffractions, etc. of the original signal via detours. Figure 1 shows an example of a reflected signal taking a detour. Depending on the time difference of the detour arriving at the sensor compared to the LOS signal and the length of the signal, these reflections have an additive effect on the overall signal strength of the received signal. This effect can have a constructive or destructive impact on the received signal, depending on the phase difference of the reflection with respect to the LOS system. [16]

The impact of this effect on the received signal can be categorized into three types:

- Type A: Partial message overlap
- Type B: Complete message overlap
- Type C: No message overlap

Since the length of a Mode S message is standardized, we can determine the timing of the detour a signal has to take, in order to belong to one of these categories [14].

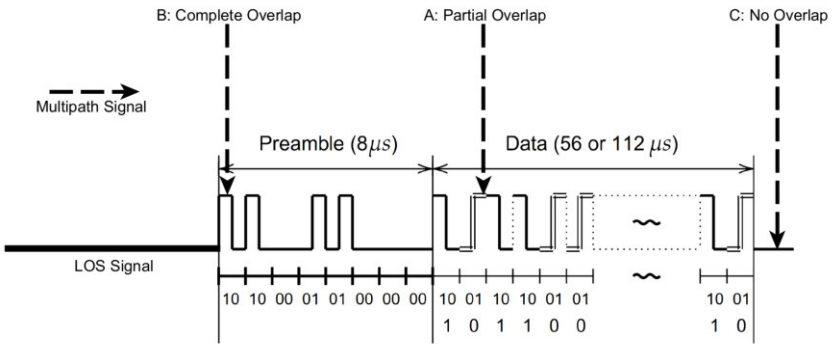

Figure 2: Three different types of influences on a received signal due to multipath propagation. The arrows highlight the point of time when the reflected signal hits the sensor (Source: Adapted Mode S reply message image from [18]).

Figure 2 shows an illustration of these three different types of multipath propagation. For instance, if the reflected signal hits the sensor within the first pulse of the LOS message, the additive effect of the multipathing effect overlaps the entire transmitted Mode S message (Type B).

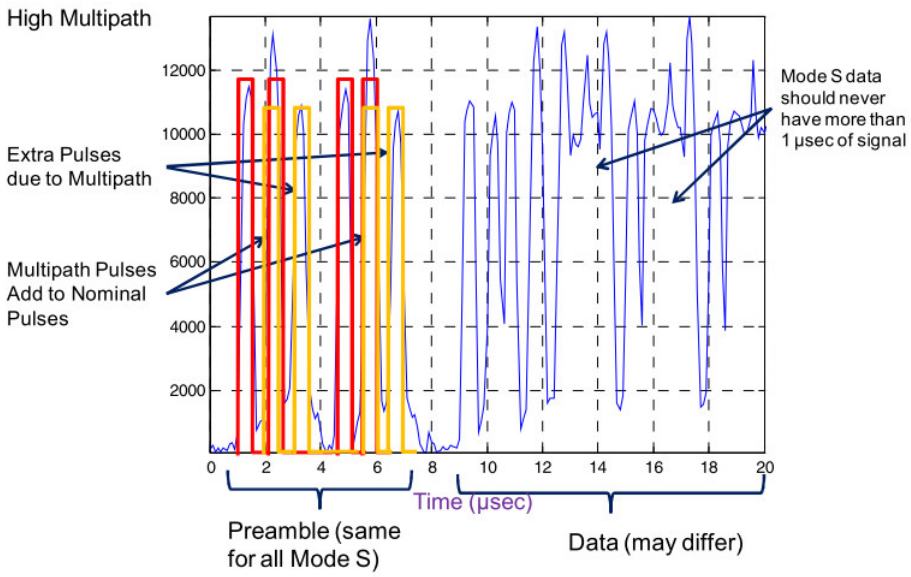

Figure 3: Mode S message signal with partial overlay - Type A (source: [2])

Figure 3 shows a real world example of the effects of multipath propagation on a received Mode S message. The yellow boxes highlight the additional pulses arriving at a later point of time than the LOS signal. This leads to an overall increased signal strength measured at the sensor.
Additionally, what also can occur and is not covered through one of the three already mentioned categories, is a blocked line-of-sight signal with only a reflected signal reaching the sensor. This results in a lower signal strength and only additional reflections having an influence on the received signal.

Since only a complete or a partial overlap of the LOS signal (Type A and B) have an influence on the received signal strength (RSS), these are the two types of effects of multipath propagation that are most interesting for the development of our model.

2.2 Influences on the received signal strength

The received signal strength (RSS) is one of the most relevant response variables of our model.
Initially, this received signal strength was used in combination with the transponder receiver distance, which can be calculated based on the encoded positions in the received airborne position messages and the known receiver positions, to calculate an expected signal strength. However, initial tests with an early version of our model, which used this simplified form of the Friis equation to determine an expected signal strength, showed very clearly that both the transmission power of the emitting transmitter as well as differences in the receiving sensors needed to be calibrated and modeled to obtain reliable and realistic results. [5] These observations resulted in three influencing variables that needed to be modeled:

1. The distance between transponder and receiver
2. The transmission power of the transponder's transmitter
3. The influence of the receiving sensor

2.2.1 Distance-induced signal attenuation

The largest part of the signal attenuation is due to the distance, whose influence can be modeled with the free space path loss model (FSPL). The IEEE defines Free Space Pass Loss as "The loss between two isotropic radiators in free space, expressed as a power ratio." [8]. More specifically the FSPL model is used to determine the loss of signal strength over distance, taking an obstacle free line of sight between the two antennas with traveling radio waves, at approximately speed of light, into account [13]. In a more mathematical way the loss over distance is defined as a decrease of $1/dist^2$, where *dist* is the distance between transmitter and receiver. When taking the speed of light and the carrier frequency into account, we get the following formula:

$$FSPL = 20 * \log_{10}(\frac{4\pi * dist * freq}{C}) \tag{1}$$

The parameter *dist* is still defined as the distance, C as the speed of light. The carrier frequency, in our case 1090 MHz, is denoted as *freq*.

2.2.2 Influence of the transmission power

The transmission power of the transponders represents another variable that must be calibrated and modeled. The strength of a transmitted signal is constant and legally restricted to the range 51 to 57 dBm [9]. Nevertheless, the actual transmission power of the transmitting transponder is unknown and dependent on the respective transponder model. Due to some exceptions, our data set may also contain transponders outside this range. To calibrate and model the influences of the different transponders contained in our data set, our model uses a developed transponder calibration algorithm described in section 4.1.2.

2.2.3 Influence of the receiving sensor

The characteristics of the receiving sensor, the so called system influence, is another crucial factor influencing the received signal strength, and therefore needs to be calibrated and modeled as well. Although the sensor network from which we obtained the data mostly uses GRX1090 sensors, also data of other sensors with slightly different hardware can be found in our data set. But even sensors of the same type have small differences, for instance different cable lengths, components from different manufacturers, or similar, which can ultimately have an influence on the received signal strength. We have therefore also developed an algorithm for this variable, which calibrates and models the characteristics of individual sensors. Further details on this sensor calibration will be provided in Section 4.1.1.

3 Description of the analyzed data set

In this work we analyze real world air traffic data. The collected messages come from a network of sensors operated by SeRo Systems GmbH. At the time of the recordings, the network consisted of 59 sensors (see Figure 4 and 5), distributed over Central Europe and the United States. The used GRX1090 sensors are specially designed for receiving Mode S and ADS-B messages and provide high precision signal and meta data. Directly after receiving, the messages are demodulated and meta data like signal strength, sensor and timestamp are added. Initially, every broadcasted Mode S message is collected by the sensor. However, for our purpose we are only interested in airborne position messages from 1090 Extended Squitters. Due to the messages being broadcasted by the aircraft, most of them are received by multiple sensors at different times and with different received signal strengths. This results in one broadcasted message leading to multiple data points in our data set.
The data is provided to us in the form of Protocol Buffer files. One file for one day of collected DF17 messages. Depending on the number of aircraft received on this day, these files have a size of about 11GB. Initially, they contain a lot of information that is not required for our analyses. However, we are only interested in some of the information broadcasted. In the first step of data handling we filter the messages and only keep the information needed. These information includes timestamp, transponder address, sensor serial, received signal strength, aircraft latitude, longitude and altitude of the sent airborne position messages. During this step, the distance between aircraft and sensor is calculated and added to the data set.
After this filtering is done, the information is again stored in the Protocol Buffer format. However, now in multiple files, partitioned on a transponder and on a sensor basis. Depending on the analysis or calculation done, either one of the partitioned formats is used. With this, the total size of the input files decreases by more than 70%.
In total, our data set contains more than 250 million different data points from just under 12.000 different aircraft transponders. A detailed description of the data is shown in Table 1. A binned coverage plot of the network in the United States can be seen in Figure 6. During our analyses, we additionally compared our results to data from other days to ensure that the observed effects were not day- or weather-dependent. These additional data sets originated from the same network of sensors but are not described here.

Figure 4: Position of sensors in Central Europe

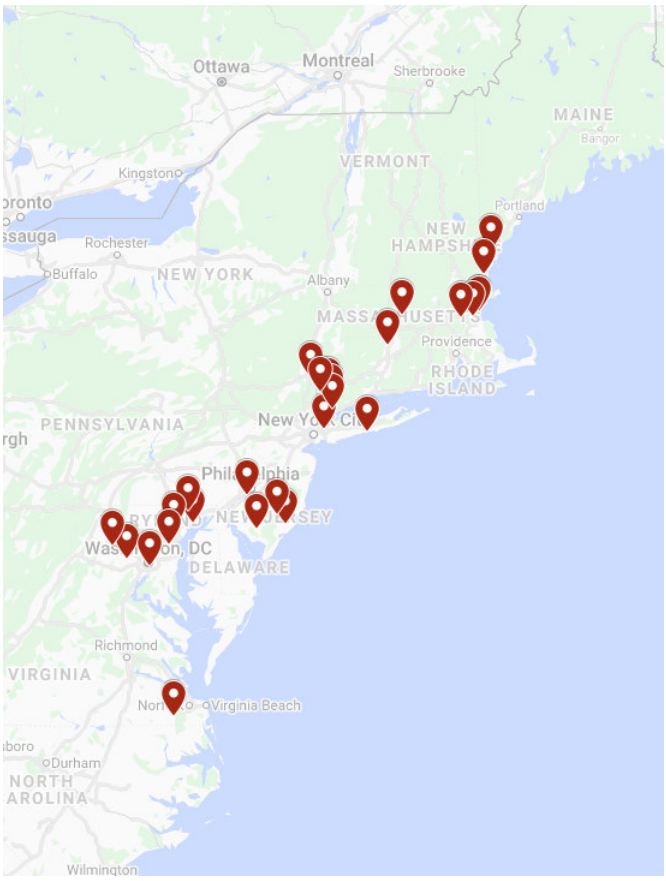

Figure 5: Position of sensors in the US

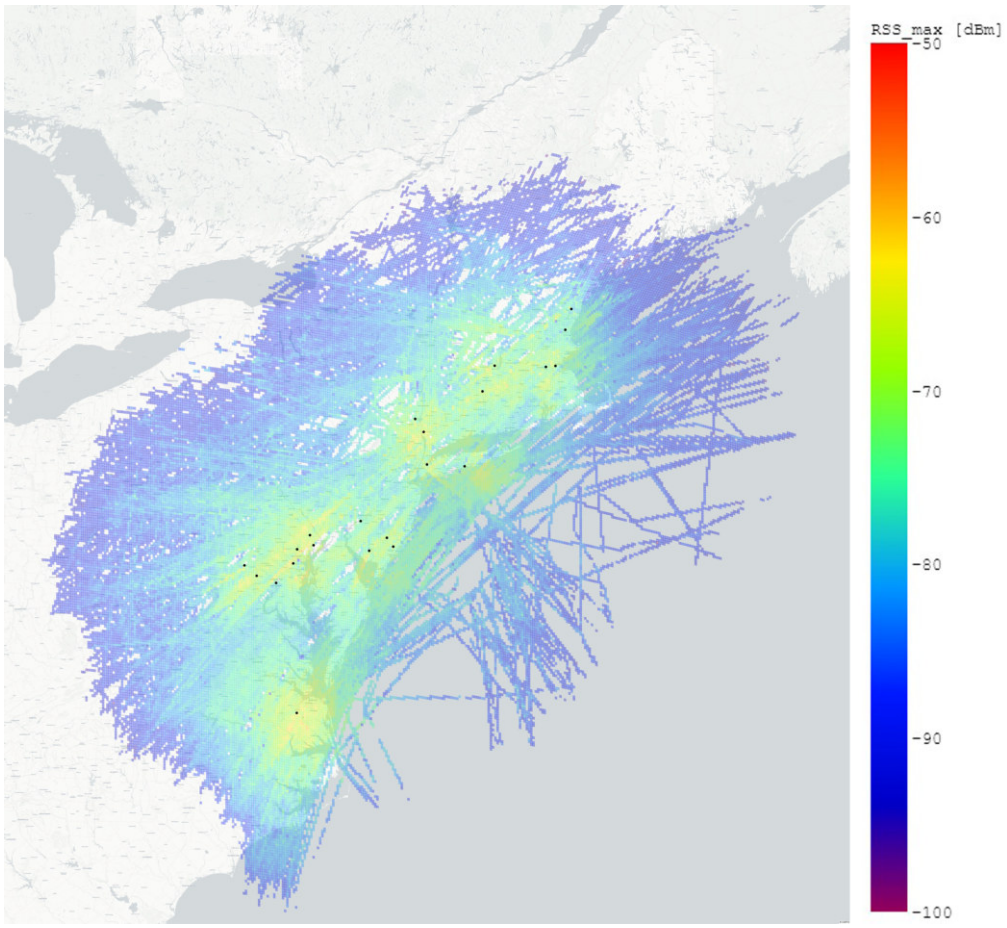

Figure 6: Coverage plot of the sensor network in the US

Input Data File	
Date	2021-11-12
Initial File Size	6.4 GB
Sensors	59
Different Aircraft	11.941
Data Points	254.304.176

Table 1: Overview of the input data file

4 Data cleansing

4.1 Developed calibration algorithms

The signal strength estimation model described in Section 2 depends on three parameters:

1. The free space path loss model
2. The transmission power of the transponder
3. The influence of the sensor

The former can be determined by known quantities, such as the frequency, the propagation speed of the wave, and the distance between sensor and transponder. In contrast, the last two parameters are unknown quantities. The transmission power of a transponder is within a specified range (min 18.5 dBW, max 27 dBW for airborne vehicles [9]), but the actual transmission power of a specific transponder is unknown. Likewise, there are variances between the influences of the different sensors, which can be attributed to the minimal device differences such as antennas with slightly different gain values or cables of different lengths and associated different resistances in the sensors themselves. In order for the model described in Section 2 to generate a good representation of the actual influence on a signal, these two parameters must be estimated as accurately as possible.
The next two sections provide a detailed description on the calibration algorithms used to estimate these unknown parameters.

4.1.1 Sensor calibration algorithm

The sensor calibration algorithm uses an estimation approach based on partitioning the data set based on sensor-transponder distances to achieve fast and accurate results.

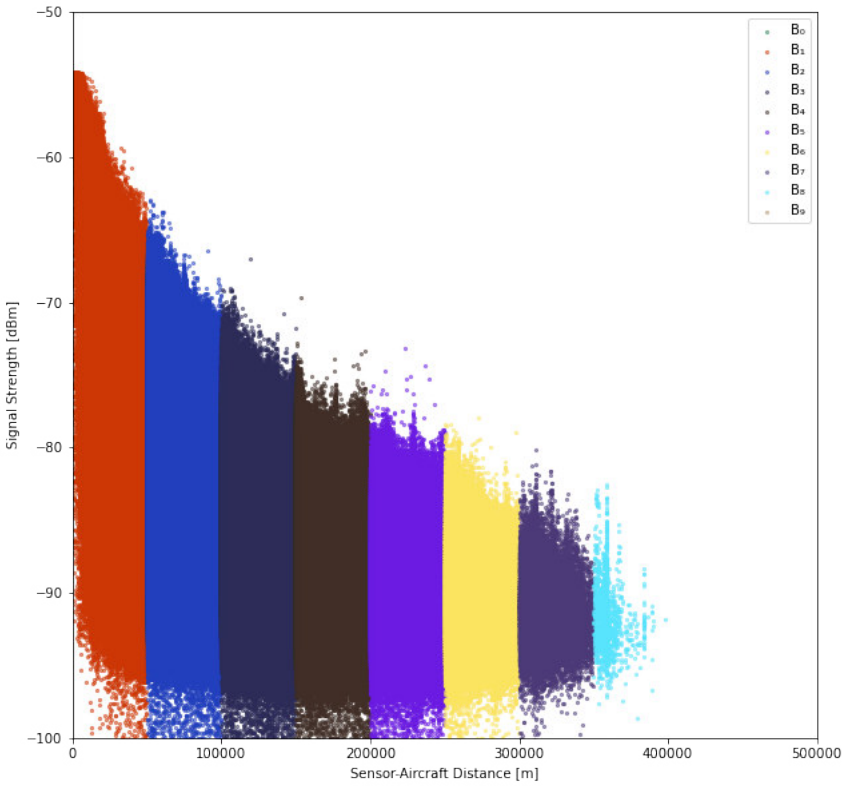

Figure 7: Simplified exemplary representation of the message partitions in the sensor calibration algorithm.

(1) In the first step, the sensor calibration algorithm partitions the messages received at a sensor based on the sensor-transponder distance into buckets B_i with a bucket size of

$$Size_B = 10km \tag{2}$$

The resulting bucket B_i is defined as

$$B_i = \{d(m) | i * Size_B \leq d(m) < (i+1) * Size_B\} \tag{3}$$

Figure 7 shows an exemplary representation of this segmentation.

(2) Receiving messages from a short distance can cause the signal strength to exceed the sensor's maximum measurable signal strength value, also referred to as clipping, in which the sensor stores the maximum measurable value ($-55dBm$) instead of the actual (indeterminable) value.

To minimize the influences of such clipping messages, the sensor calibration algorithm ignores all messages with a sensor-transponder distance $d < 50km$, which corresponds to the messages in buckets $\sum_{i=0}^{4} B_i$

(3) In order to prevent the calibration result from being distorted by sparsely populated buckets, the algorithm also ignores buckets with a message population smaller than 75% of the average bucket population.

(4) For all other buckets, the algorithm calculates a reference value RSS_{Ref} which is described as

$$RSS_{Ref} = FSPL - TP_{Max} + P_{99}(RSS_{Ref}) \tag{4}$$

where TP_{Max} refers to the maximum specified transmission power of 57 dBm (or 27 dBw) defined [9], P_{99} refers to the 99-percentile of the reference values RSS_{Ref} and $FSPL$ refers to the free space path loss model which is defined as

$$FSPL = 20 * \log_{10}(\frac{4\pi * dist * freq}{C}) \tag{5}$$

where $dist$ refers to the sensor-transponder distance, $freq$ refers to the frequency (here 1090 MHz), and C to the speed of light [9].

(5) The algorithm then aggregates these reference values of the relevant buckets $RSS_{ref,rel}$ as

$$Influence_{sensor} = Median(RSS_{ref,rel}) \tag{6}$$

which represents the estimated influence of the individual sensor. This influence of a sensor is usually positive (gain), due to the gain of attached antenna, but can also be negative (loss). This influence is removed in the following processing steps in order to obtain values that are comparable between different sensors.

4.1.2 Transponder calibration algorithm

Similar to the sensor calibration algorithm, the transponder calibration algorithm uses a combination of known quantities to estimate an unknown quantity, the transmission power of a specific transponder.

(1) In the first step, the algorithm determines the estimated transmission power for each message. This estimated transmission power TP_{Est} is defined as

$$TP_{Est} = RSS - Gain + FSPL \tag{7}$$

where RSS refers to the received signal strength of the message, $Gain$ refers to the influence of the corresponding sensor estimated by the sensor calibration algorithm described in Section 4.1.1, and $FSPL$ refers to the Free Space Path Loss Model (see equation (5)).

(2) In the second step, the algorithm determines the deviation $Dev_{Max,Est}$ defined as

$$Dev_{Max,Est} = |TP_{Max} - TP_{Est}| \tag{8}$$

which represents the absolute difference of the estimated transmission power TP_{Est} determined in equation (7) and the maximum specified transmission power of 57 dBm (or 27 dBw) defined in Annex 10 to the Convention on International Civil Aviation for each message [9].

(3) In the next step, the algorithm partitions the messages based on the corresponding transponder addresses and estimates the transmission power for each of these addresses based on the list of corresponding deviations $Devs_{address}$.
The resulting estimated transmission power of a transponder $TP_{Est,address}$ is defined as

$$TP_{Est,address} = TP_{Max} - P_{99}(Devs_{address}) \tag{9}$$

4.2 Filtering of the analyzed data set

The data set description in Section 3 shows, that there is the need to process and analyze the huge amount of data. Hence, we implemented filters to reduce the data set to the most relevant messages for our analysis. The data set was filtered with the following set of filters in given order:

1. Flight Level Filter
2. Noise detection
3. Radio Horizon Filter
4. Antenna Filter

Each filter will be explained in the next sections like the following: First we start with some theoretical background of the filter and why it is needed. This is followed by a short description on the used settings for this filtering. Also the amount of filtered messages, for improved overview, is provided.

4.2.1 Flight level filter

First, we start with the Flight Level Filter, which enables us to set a range of so called Flight Levels to analyze. A Flight Level is a level in altitude with a constant atmospheric pressure in relation to a specific pressure datum, defined by the FAA [4]. Flight Levels are denoted in 100 feet, like FL250 is an altitude of 25,000 feet. Therefore we also used the barometric height in the received messages, to comply with the altitude measured by the atmospheric pressure.

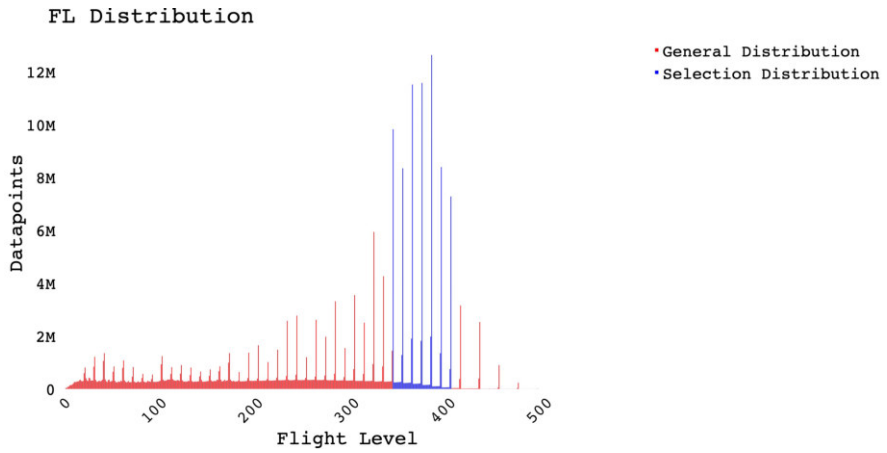

Figure 8: Flight level distribution in the data set, selected Flight Levels are denoted in blue

With the help of this filter we only consider aircraft at cruising altitude and thus prevent problems, such as clipping, with landing or taking off aircraft.
In the present analysis, as shown in Figure 8, we only considered the FL340 (10,350 meters) to FL400 (12,200 meters), which is a good distribution of cruising altitude compared to Figure 8. This leads us to a reduction of 165,642,695 messages in our data set, which is a reduction by 65.14%.

4.2.2 Noise detection

The Noise detection is used for checking the viability of messages grouped into windows within our data set, on a higher level. The algorithm itself is implemented in a recursive manner, starting with the check if the window is valid. Valid in this case was defined as a maximum of 100 messages per window, so it is feasible to check. If the window was too large (more than 100 messages), it was split into two equally distributed windows - checked again, leading to the recursive implementation. Using valid windows, the algorithm checks whether the reception rate is in a predefined acceptable range. This was defined as a minimum of 2 messages per second minus a, previously defined, maximum loss of 65%. The minimum of 2 messages relies on the fact, that we only considered

position messages. Summarizing the algorithm consists of the following two parts:

(1) Window size: Splitting the window size until it contains less than 100 messages

(2) Reception rate: Checking if the window contains at least 2 messages per second, having a maximum loss of 65% in mind

As a result 34,117,607 messages were removed from out data set. This is a reduction by 13.42% of the initial data set, and a reduction by 38.48% after the flight level filter.

4.2.3 Radio horizon filter

After the data set is filtered for a specific Flight Level range, which is relevant for us, and the Noise detection filtered messages which would interfere our analyses, we now want to detect outliers using the Radio Horizon.
The communication of messages presented in this work is based on radio waves, which limits it to certain physical properties. One of them is the so called Radio Horizon, with which the maximum range of a 1090 MHz radio receiver (or transmitter) can be determined. Assuming the earth to be a perfect sphere, the horizon distance from a receiver can be calculated by applying the Pythagorean Theorem [11]. Letting d be the horizon distance, R the radius of Earth, h the receiver altitude and assuming that $h \ll R$. The properties of electromagnetic waves, not traveling in straight lines, is determined using the factor k:

$$RH = \sqrt{2 * k * R * h} \tag{10}$$

With $k = \frac{4}{3}$ the earth radius is adjusted in order to include the bending of radio waves towards the horizon. This is merely an approximation and the perfect value for k changes with factors like altitude, frequency etc. However, this is sufficient for our purpose [3]. By inserting the known values for R and k we obtain the following equation:

$$RH = 4.12 * \sqrt{h} \tag{11}$$

The height in our case is given by the addition of sensor and transponder altitude - leading to the Radio Horizon formula as following:

$$RH = 4.12 * (\sqrt{SensorAlt} + \sqrt{TransponderAlt}) \tag{12}$$

We now use this formula to calculate the Radio Horizon for each message and remove them if, and only if the measured distance is larger than the Radio Horizon subtracted by a predefined threshold of 30km (Equation 13). Resulting in a removal of 2,137 messages, which cannot be correct as they would undermine physical properties and therefore removing 0.0008% of the initial data set and 0.003% since the Noise detection.

$$dist > RH - 30km \tag{13}$$

4.2.4 Antenna filter

Except for light aircraft, aircraft usually send a signal from two different antennas. Whilst the top antenna results in a good signal strength when the aircraft is on the ground, the bottom one has its benefits, regarding signal strength, in the air. This is depending on the line of sight theory, because the top antenna is blocked by the aircraft itself whilst being on cruise level. As we filtered our data set to Flight Levels, which are on this altitude, the bottom antenna is the more relevant one for us. As the received messages are sent from alternating top and bottom antenna, there was a need to filter only for the bottom ones, to further dense the data set.
Our classification of antennas works in a recursive manner, using the window size which is given by time. There are three methods which are prerequisites for the following explanation of the algorithm:

(1) **hasAcceptableLoss:** Returns *True* if the loss within the window is less than 60%. The loss itself is defined as the ratio between expected position messages (2 per second) and the actual received ones.

(2) **isTooLargeToClassify**: Returns *True* if there are more than 100 messages within a window. *False* if not.

(3) **isSplittable**: A window is called *splittable*, if there are more than 20 messages within the given window, which results as *True* of this method.

As initial window the complete recorded signal of one transponder sensor combination is used. The following algorithm is then used to determine by which antenna a message was sent:

(1) If the window has no acceptable loss and is not splittable, all signals, within the given window, get classified as unknown due to a too small amount of data

(2) In case of a too large window with an acceptable amount of loss, the window gets split in half and the algorithm starts from the beginning (recursive)

(3) When the window is not too large to classify and has an acceptable amount of loss, the actual classification can be started:

(3.1) Statistical values, such as min max and mean, are determined

(3.2) The values of each message get normalized in a mathematical manner between -1 (highest RSS) and 1 (lowest RSS) within the window like the following:

(3.2.1) If RSS is greater than the mean:

$$indicator = abs(RSS - mean)/abs(max - mean) \tag{14}$$

(3.2.2) If not:

$$indicator = -1 * abs(mean - RSS)/abs(mean - min) \tag{15}$$

(3.3) Depending on the normalized indicator per message within the window, the following classification is done:

(3.3.1) Top antenna: $indicator \geq 0.15$

(3.3.2) Bottom antenna: $indicator \leq$ -0.15

(3.3.3) Unknown antenna: -0.15 $< indicator <$ 0.15

The classified result was used to select only the bottom antenna for further analysis, like described. This leads to a reduction by 21,385,242 messages in our data set.
This results in a reduction of 21,385,242 messages from the data set, which corresponds to 8.41% from the initial data set and 39.21% since the Radio Horizon Filter.

In the following section, the filtered and classified data set will wrapped up, to point out differences between the initial data set and the filtered one.

4.3 Filtered data set

As described in Section 3 the initial data set contains 254.304.176 messages. Applying the introduced filters, 86.96% (221.147.681) of these messages are filtered. The resulting 13.04% (33.156.495) messages are analyzed in the following sections. Figure 9 shows the distribution of received messages at the different sensors: the red bars highlight the proportion of remaining messages per sensor. Since not all sensors of the sensor network were online on the day of recording, the data set analyzed here contains data from only 46 of the 58 sensors. Additionally, a few receivers have a very low amount of data points. The reason for this are some testing receivers with a very limited reception area present in the network. From these devices, almost all data points are filtered out.

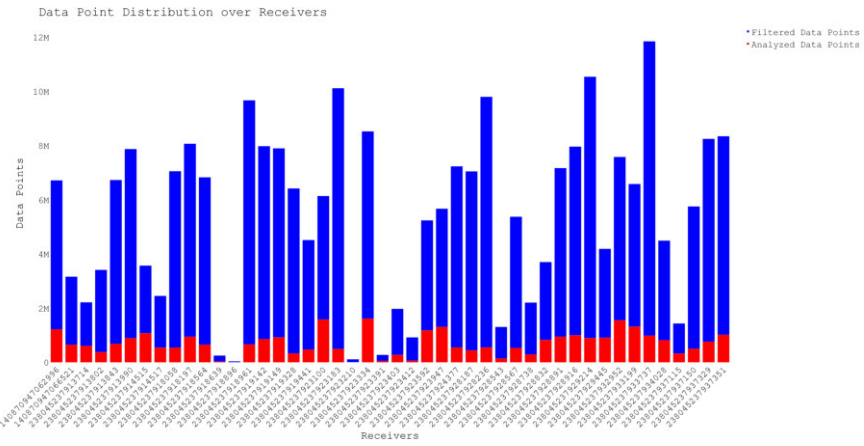

Figure 9: Data point distribution among sensors

5 Analysis

After filtering our data set we want to start exploring it in a graphical way. Because it is not feasible to plot every single data point onto a map, due to performance constraints of map libraries, we needed to aggregate data points into geographical groups, our so called cells.
There is already an existing geographical binning library by *Google - "S2 Geometry"* (short S2) [7]. S2 provides an API to group data points by different levels in size of geographical cells. The levels are defined between 0, which is the largest cell size in a geographical matter, and 30, consequently the smallest cell size [6]. To determine which message of our data set relate to which cell in S2, we use the longitude and latitude of the aircraft in the received message.

Cell level	11
Min. area	12.18 km^2
Average area	20.27 km^2
Max. area	25.52 km^2
Min. cell edge length	3 km
Max. cell edge length	5 km
Number of cells (covering the world)	25M

Table 2: Used configuration of *Google - S2 Geometry*

For our geographical analysis of our data, we've used the cell size 11 (denoted in Table 2), resulting in a covered area between 12.18 km^2 and 25.51 km^2, given average by S2 is 20.27 km^2. The edge lengths vary between 3 to 5 km [6].
In the following subsection we will further elaborate the plots, used for our geographical analysis.

5.1 Coverage

While iterating over each message in our data set, we assign them to their geographical cell using S2, like described beforehand. Next to the cell identifier, the receiver serial is also extracted. Pairing this data, we can plot it onto a map per receiver, using the S2 cell to de-clutter the view instead of plotting each single data point. For better insight into our data, the received signal strength of each cell will be visualized in the plot. To determine the color scale, we save and show the maximum received signal strength for each cell-receiver paring. An example of a coverage plot can be seen in Figure 10.

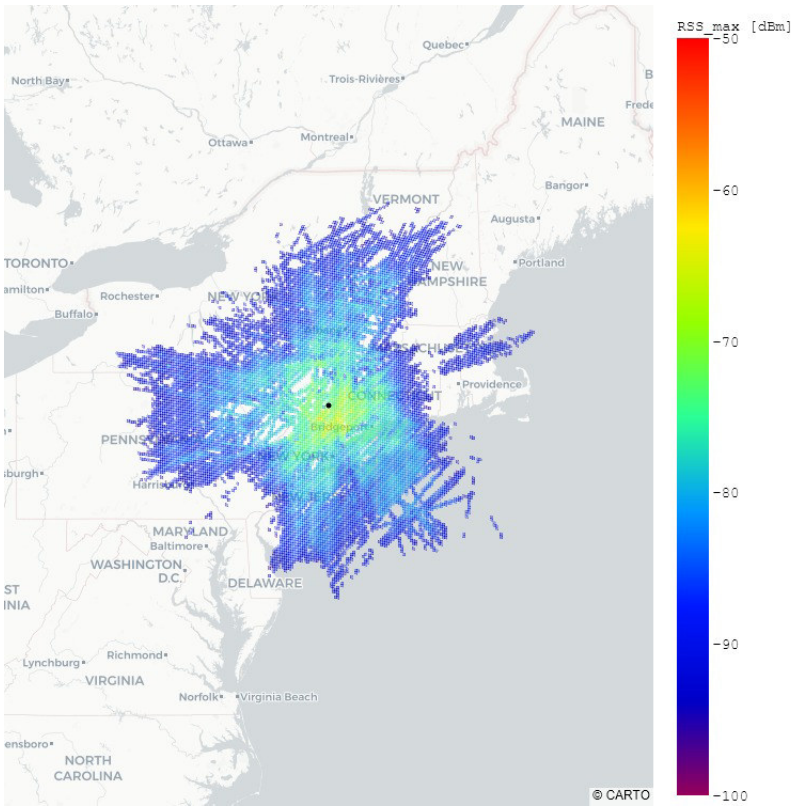

Figure 10: Coverage plot of receiver 238045237913843

To conclude, this gives a better understanding of the covered area by each sensor, as well as some insight into the received signal strength for different geographical locations. Those different signal strength per location can therefore also be combined with some geographical open source intelligence, to identify areas which could lead to multipath or other effects from geographical conditions (e.g. mountains, skyscrapers, . . .).

5.2 Received vs. expected signal strength

Another interesting measure to validate our model against the real data in the data set described in Section 3, is to examine the deviation between the signal strength expected by our model and the measured signal strength. A position-independent, constant deviation between the expectation and the actual measured values, could indicate that the model does not consider all influences affecting a real signal and thus constantly overestimates the signal strength. However, deviations that are clearly position-dependent would be particularly interesting here, since these could be an indicator of multipath propagation.

The deviation in received and expected signal strength for a specific sensor is calculated in 4 steps:

(1) For each message received at the sensor, the expected signal strength is calculated based on the calibration result for the sensor, the calibration result of the transponder's transmitter and the distance between transponder and sensor.

(2) Each message is assigned to its covering S2 [7] cell at level 11 [6]

(3) We calculate the median received signal strength and the median expected signal strength for each S2 cell we received messages from.

(4) The deviation for each of these cells is then calculated as the difference of the median received and the median expected signal strength.

6 Results

The analysis of the data set revealed that the model described in Section 2 is not a perfect representation of reality. The analysis of the data at the different sensors revealed an interesting distribution of the deviation between expected and received signal strength, which is shown in Figure 11.

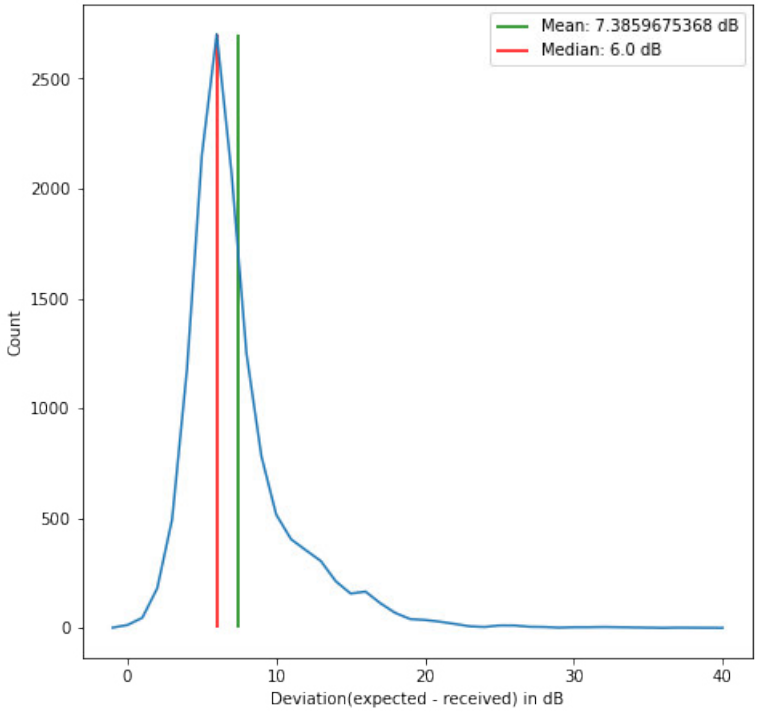

Figure 11: Distribution of the deviation between expected and received signal strength

As already mentioned in the previous section, such a relatively constant deviation of our model indicates that the model does not consider one or multiple factors that in reality have a relatively constant influence on the strength of a signal. Regardless of this relatively constant deviation, the analysis of the data set nevertheless revealed some interesting patterns, which we present in the following subsections categorized form.

6.1 The expected results

As a starting point we can look at a nearly perfect, expected result. Like shown Figure 12, the sensor has a good coverage. Notable here is, the round propagation of signals which shows a good coverage in all direction in every angle.

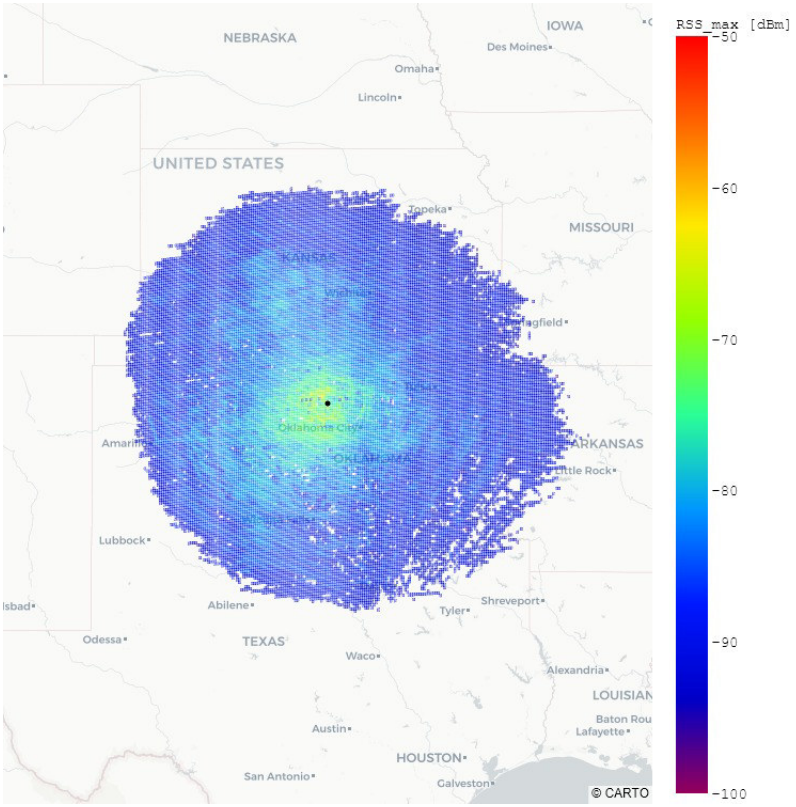

Figure 12: Received signal strength plot for an expected example (Sensor: 238045237923334)

Furthermore the deviations are also on a low level, denoting good results, as one can see in Figure 13 and Figure 14.

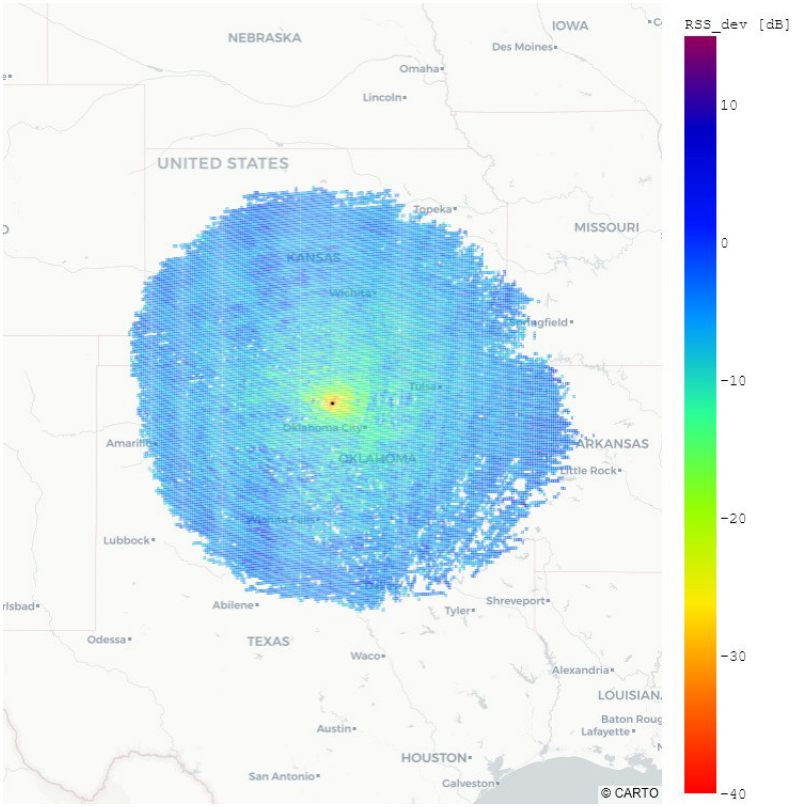

Figure 13: Plot for deviation between expected and received signal strength for an expected example (Sensor: 238045237923334)

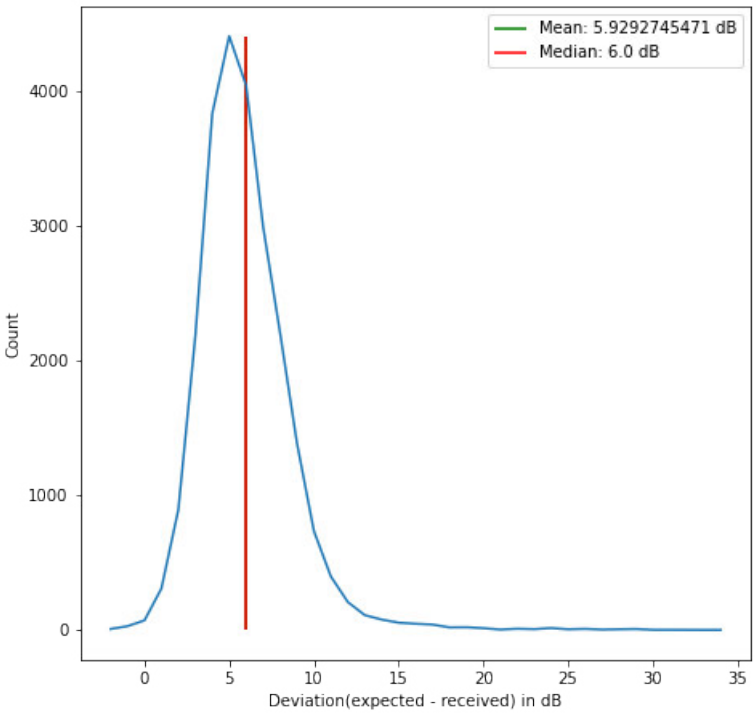

Figure 14: Distribution of the deviation between expected and received signal strength Sensor: 238045237923334

Regarding the calibration, Figure 15 shows a good alignment of data points with the Free Space Path Loss model used as a bases for our model described in subsubsection 2.2.1. The only problem one can see are messages which are above the reception threshold (about -55dBm), so called clipping. In a more visual way, the first meters (x-axes) in Figure 15 are a straight line. This means, that the messages were received louder than the sensors can measure, leading to data points at max reception rate. Therefore the received signal strength is "clipped".

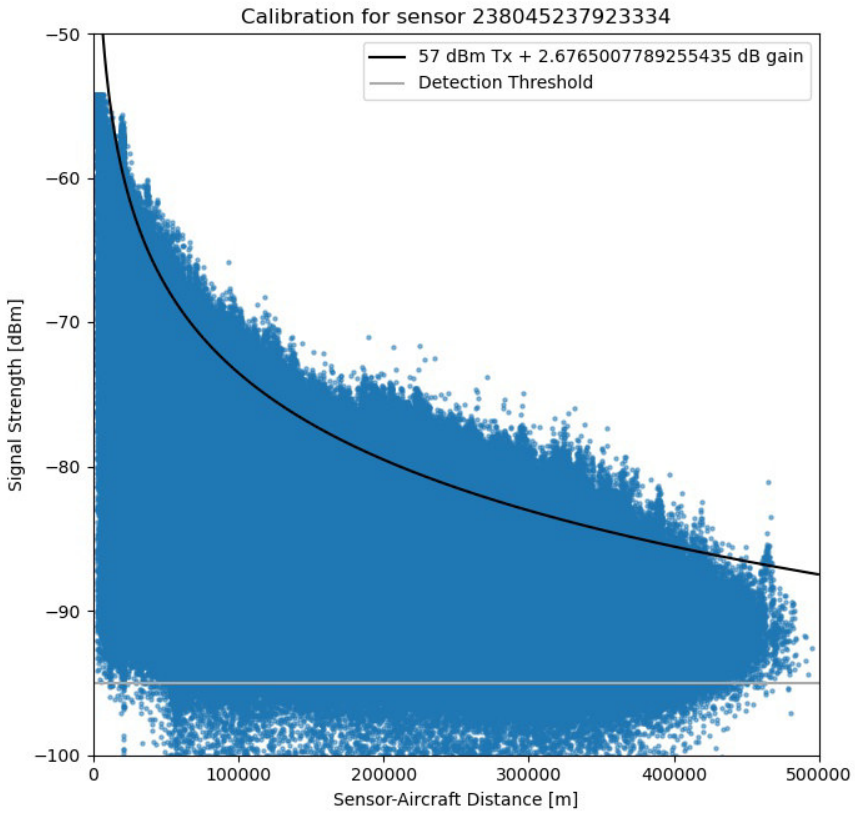

Figure 15: Calibration plot of an expected, real example

Due to the fact, that reality is rarely near as perfect as the previous example, the following section will introduce different types of effects, which lead to deviating results.

6.2 Observed effects

Like mentioned before, we also found various effects, which deviate from our expected results and therefore need an in depth explanation. The subsequent sections will examine the following categorized effects:

- Obstructions
- Beams
- Halos

6.2.1 Obstructions

The first and easiest effect to explain are obstructions, i.e. local conditions that strongly weaken or completely block the signal. Therefore those effects are already visible on our coverage plots like Figure 16.

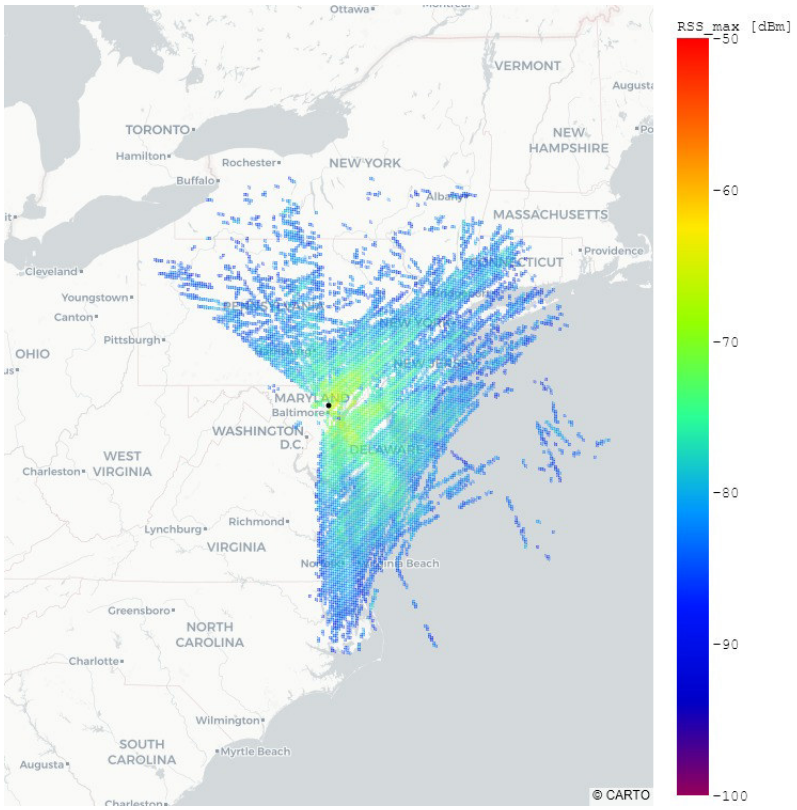

Figure 16: Obstructed coverage by building (Sensor: 238045237928187)

The coverage plot shows a big gap in missing signals from south, south west. This effect is easily explainable, using Open Source Intelligence (OSInt) when we look at the building where the sensor is placed, based on given position data. Using longitude, latitude as well as a rough altitude estimate and check the location using Google Earth, we get the following result:

Figure 17: Building blocking receiving signals for sensor 238045237928187 (Image data by Google Earth)

The yellow marker indicates, that the sensor is probably placed on the front side of the building, from this perspective. As the sensor is not on top, it will be blocked by the buildings structure, leading to the given signal loss in various directions.
Next to this quite obvious example, there are many more areas in our coverage plots which can be explained by different environmental circumstances. For example in Figure 18, which represents the RSS deviation plot, one can see that local environmental conditions, such as in this case larger mountain ranges, also lead to deviations in the RSS. Like shown in the plot, there are higher amounts of deviations near to the complete lack of signal, especially in the north.

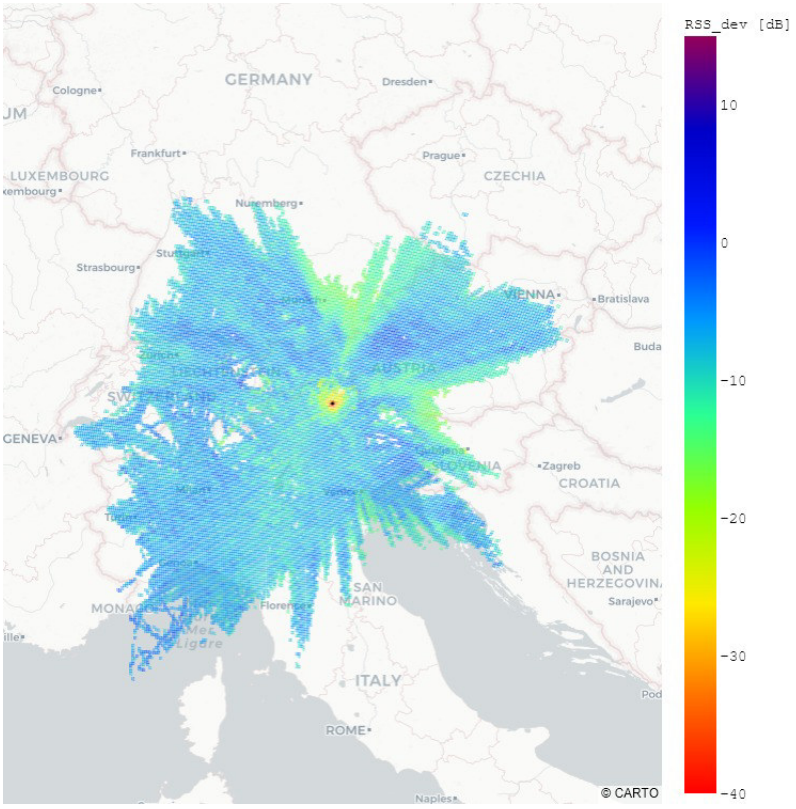

Figure 18: RSS deviations based on obstructions (Sensor: 238045237923100)

6.2.2 Beams

On some sensors we furthermore observed a pattern we call beams. These beams are visible as a steady constant attenuation of the signal strength starting near the sensor and increasing outwards. One example is shown in Figure 19. These beams, however, can be differentiated between wide and narrow beams. The wider beams, as for instance in Figure 19, can be explained when observing the environment the sensor is located in. In these cases, there are always objects such as trees, which do not completely block the signal strength, but attenuate it in the corresponding direction. Most likely by intruding the Fresnel zone between transponder and sensor [15].

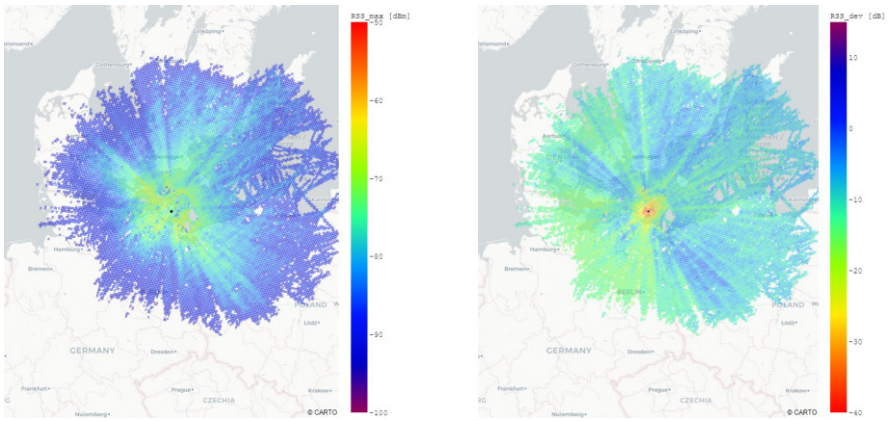

(a) Coverage (b) RSS Deviation

Figure 19: Beams in the RSS

However, there are some narrow beams, shown for instance in Figure 20, that cannot be explained by checking the sensors environment. If these beams were caused by the attenuation of the signal through objects standing in the field of view, the result would be much wider with an outwardly increasing width, more like in the first Figure. In our data there are even sensors which are located in a wind farm off the coast with a near perfect reception area that show these narrow beams.

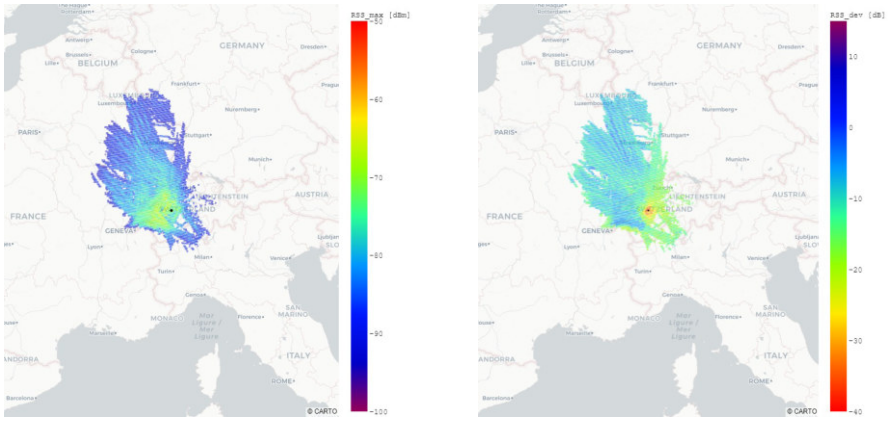

(a) Coverage (b) RSS Deviation

Figure 20: Narrow beams in the RSS

6.2.3 Halos

Another interesting effect, which we will call halos in the following, can be described by ring-shaped signal strength anomalies around the sensors.

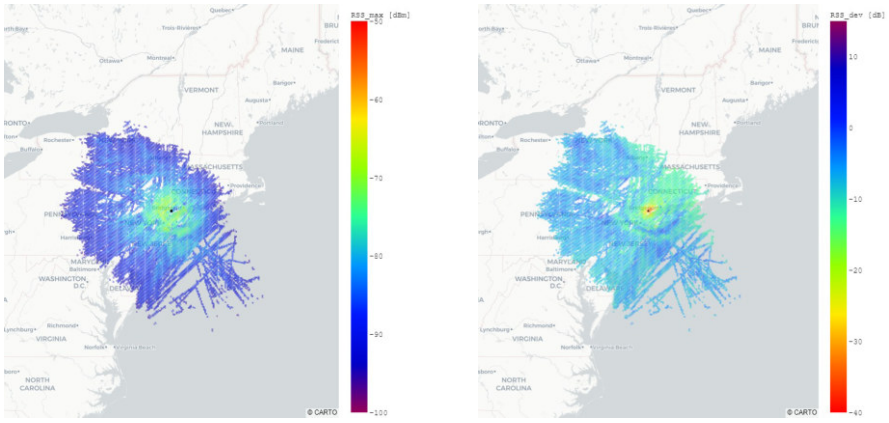

(a) Coverage (b) RSS Deviation

Figure 21: Halo of sensor 238045237918961

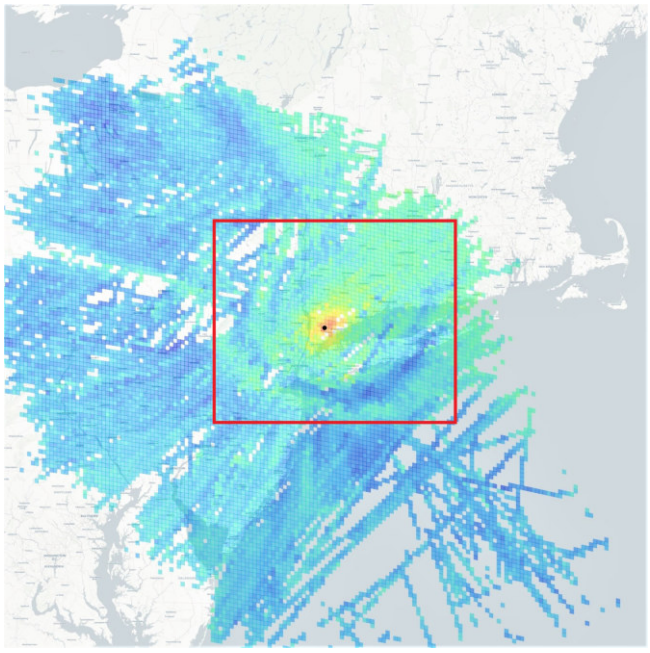

Figure 22: Highlighted deviation of sensor 238045237918961

Figure 21 shows such an exemplary anomaly, which was observed for a total of three out of 59 sensors in our data set. It is unclear what causes these halos, but since the three affected sensors are the same sensor model at different locations (both in Europe and the US), it is reasonable to assume that the geographic conditions at the sensor's location are responsible for the signal strength anomaly.
The first sensor, shown in Figure 21 and Figure 22, is placed directly at the Westchester Country Airport in Westchester County, New York, US. Its immediate surroundings are thus characterized by large, flat concrete surfaces (the runways) and unbuilt terrain.

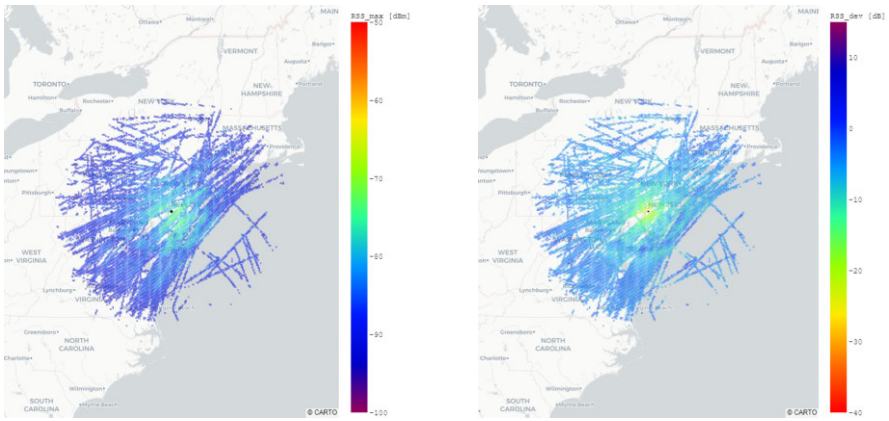

(a) Coverage (b) RSS Deviation

Figure 23: Halo of sensor 238045237919328

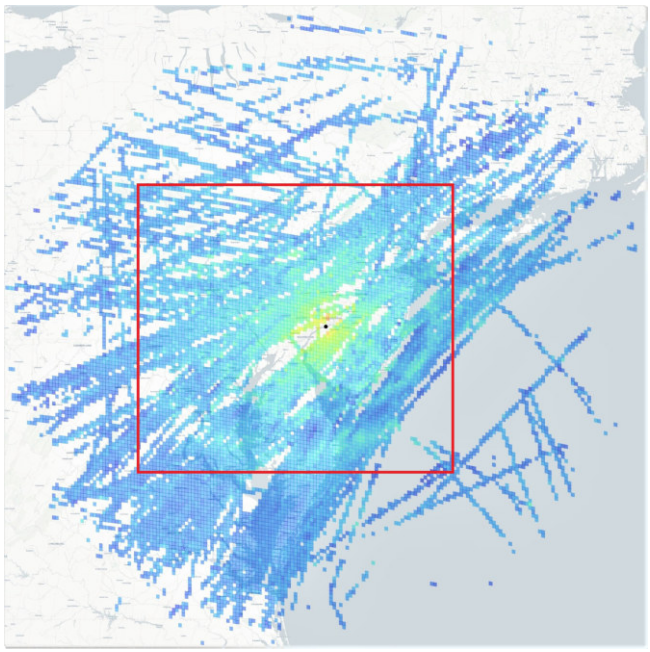

Figure 24: Highlighted deviation of sensor 238045237919328

The second sensor, shown in in Figure 23 and Figure 24, is, similar to the first one, placed directly next to a runway at the Philadelphia International Airport in Philadelphia, Pennsylvania, US. Its immediate surroundings are thus also characterized by large, flat concrete surfaces (the runways) and unbuilt terrain. Also, the sensor is placed right next the Deleware River, which is another flat surface in close proximity to the sensor. The geographic features in the immediate vicinity of the sensor are almost completely consistent with those of the first sensor, suggesting a relationship between the anomalies and the proximity to an airport.

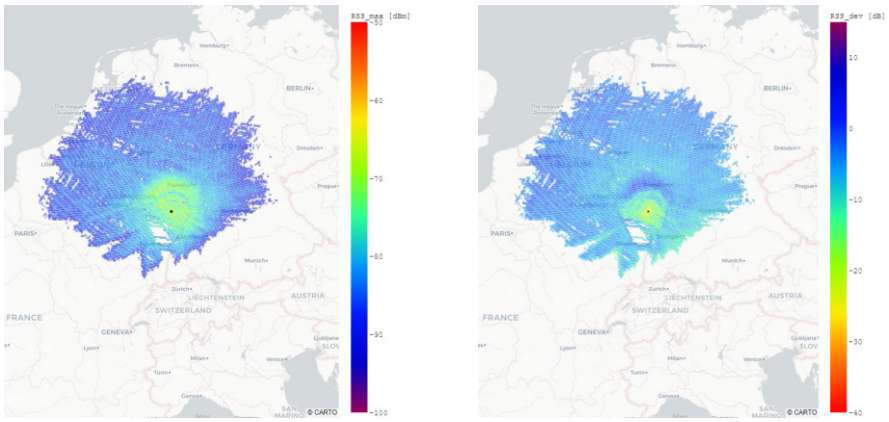

(a) Coverage (b) RSS Deviation

Figure 25: Halo of sensor 238045237934028

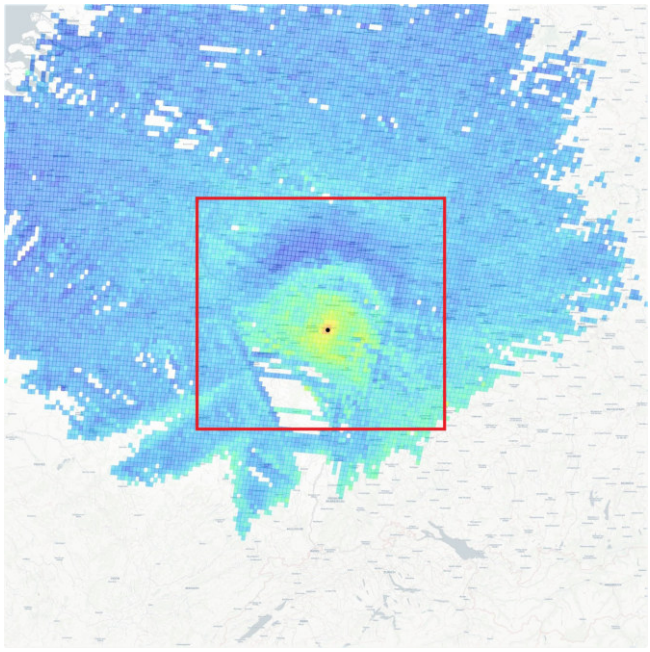

Figure 26: Highlighted deviation of sensor 238045237934028

The third and final sensor affected by these halos, shown in Figure 25 and Figure 26, is located on the rooftop of a building at the Technical University of Kaiserlautern in Kaiserslautern, Germany. Its immediate surroundings are a university campus, which like the larger surrounding area, is heavily tree and forest dominated. It is not located next to an airport (the nearest airport is Ramstein Airbase, which is about 11 km away), but is located directly next to a helipad, which is also a large concrete surface in the immediate vicinity of the sensor.

7 Conclusion

The goal of this work was to develop a model that allows an accurate calculation of the expected signal strengths. Based on the Friies-Equation and the FSPL-model, a new model was developed, which determines the influences of location-independent effects, such as the influence of the sensor, the fixed but unknown transmission strength of the transmitter, as well as the unknown antenna position of the transmitter by means of various developed calibration algorithms, in order to identify geographical clusters of deviations.

The first and most common pattern revealed by the model is a classic shadowing of the sensor by objects in the immediate vicinity. This shadowing often occurs in unexposed sensors whose reception range is restricted by buildings or other non-permeable objects at a short distance. These shadowing of sensors are expected effects, which could be modeled as such using appropriate terrain data, but this is beyond the scope of a classical line-of-sight model. Besides this classic shadowing another pattern, which can be described by beam-shaped deviations in signal strength around a sensor, was revealed. Some of these beam-shaped deviations, especially those with wider beams, can often be explained by the immediate environment of the sensor, for example partial shadowing or attenuation of the signal from one direction by trees or similar objects. In our analysis, deviations with narrow beams cannot be explained by the objects in the immediate environment and also occur with totally exposed sensors in offshore wind farms. These deviations with narrow beam patterns cannot be explained with our methods and could be an effect of multipath propagation. The third and probably most interesting pattern can be described by ring-shaped deviations, so-called halos, at medium distance around a sensor. This phenomenon was discovered at three sensors with relatively similar close environments. The first two sensors are located in close proximity to airports, their direct environment therefore characterized by large concrete surfaces (the runways). The third sensor is located in a more rural setting, but is located right next to a helipad, so its immediate environment is also dominated by a large concrete surface. This leads to the conclusion that large concrete surfaces in close proximity to the sensor could be responsible for these halos. Furthermore, it is noticeable that the anomaly at sensor 238045237934028 is pronounced differently, which could be due to the different shape and size of the concrete surface at the sensor.

Although the deviations determined by our model averaged out at 7.4 dB (median 6.0 dB) - shown in Figure 11 - they deviate strongly for some sensors.

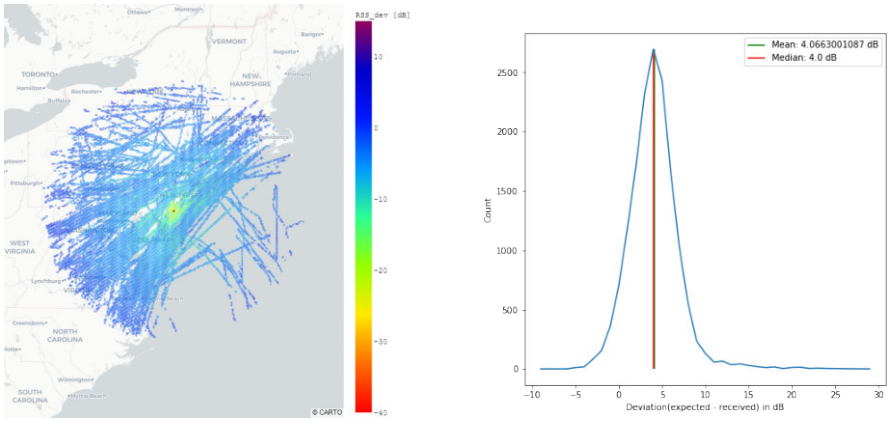

(a) Geographical deviation representation (b) Deviation Histogram

Figure 27: Deviation of sensor 238045237923183

Figure 27 shows a geographical representation as well as a histogram of the deviations at sensor 238045237923183. Sensor 238045237923183 shows a relatively small deviation averaging out at 4.1 dB (median 4.0 dB). The determined deviations are almost exclusively at a short distance for this sensor and could be due to clipping of the sensor. The determined deviation is therefore most probably just a calibration error.

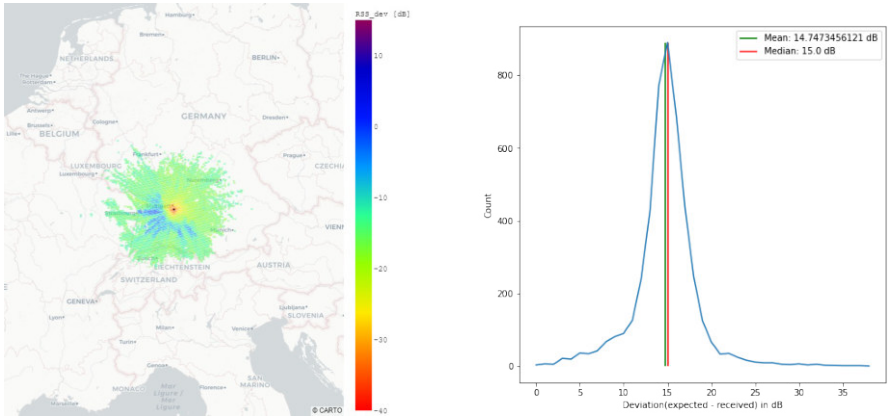

(a) Geographical deviation representation (b) Deviation Histogram

Figure 28: Deviation of sensor 238045237937115

Figure 28 shows a geographical representation as well as a histogram of the deviations at sensor 238045237937115. Sensor 238045237937115 shows a relatively high deviation averaging out at 14.7 dB (median 15 dB). In contrast to sensor 238045237923183, the deviation at this sensor is conspicuously distributed and not purely due to clipping effects.

Although we verified our results by comparing them with data obtained on another day, confirmation of our results with data collected over a longer period of time is planned for future work. Additionally, we want to further investigate the observed results, especially the narrow beam and halo shapes probably due to the effects of multipath propagation.

8 Bibliography

[1] Commission implementing regulation (eu) no 1207/2011. *Official Journal of the European Union*, 2011.

[2] Yu Hsuan Chen, Sherman Lo, Per Enge, and Shau Shiun Jan. Evaluation amp; comparison of ranging using universal access transceiver (uat) and 1090 mhz mode s extended squitter (mode s es). In *2014 IEEE/ION Position, Location and Navigation Symposium - PLANS 2014*, pages 915–925, 2014.

[3] Armin W Doerry. Earth curvature and atmospheric refraction effects on radar signal propagation. *Sandia Report SAND2012-10690*, 2013.

[4] Federal Aviation Administration (FAA). Pilot/controller glossary, 2018. `https://www.faa.gov/air_traffic/publications/media/pcg_basic_chgs%201_2_9-13-18.pdf`.

[5] H.T. Friis. A note on a simple transmission formula. *Proceedings of the IRE*, 34(5):254–256, 1946.

[6] S2 Geometry. S2 cell statistics, 2021. `https://s2geometry.io/resources/s2cell_statistics.html`.

[7] S2 Geometry. S2 geometry, 2021. `https://s2geometry.io/`.

[8] IEEE. Ieee standard for definitions of terms for antennas. *IEEE Std 145-2013 (Revision of IEEE Std 145-1993)*, pages 1–50, 2014.

[9] International Civil Aviation Organization. Annex 10 to the Convention on International Civil Aviation. Volume IV: Surveillance Radar and Collision Avoidance Systems, 2007.

[10] Markus Irsigler. *Multipath Propagation, Mitigation and Monitoring in the Light of Galileo and the Modernized GPS*. Dissertation, Universität der Bundeswehr München, Fakultät für Luft- und Raumfahrttechnik, Neubiberg, 2008.

[11] Bob Kibble. How big is the earth? a calculation beyond your horizon. *Physics Education*, 46(6):685, 2011.

[12] Kevin McClaning. *Wireless Receiver Design for Digital Communications* -. Institution of Engineering and Technology, London, 2012.

[13] John H. Mott and Darcy M. Bullock. Estimation of aircraft operations at airports using mode-c signal strength information. *IEEE Transactions on Intelligent Transportation Systems*, 19(3):677–686, 2018.

[14] International Civil Aviation Organization. Technical provisions for mode s services and extended squitter, 2018.

[15] J.D. Parsons. *The Mobile Radio Propagation Channel*. John Wiley & Sons, Ltd, 2001.

[16] Pavel Puričer. *ADS-B signal processing improvement in difficult environment*. Dissertation, Czech Technical University in Prague, 2019.

[17] C. Siller. Multipath propagation. *IEEE Communications Magazine*, 22(2):6–15, 1984.

[18] Junzi Sun. *The 1090 Megahertz Riddle: A Guide to Decoding Mode S and ADS-B Signals*. TU Delft OPEN Publishing, 2 edition, 2021.